The stimulated Raman threshold. I. Experiment

Behrouz Amini[a] and Francis F. Chen[b]
University of California, Los Angeles, California 90024

(Received 21 October 1985; accepted 12 August 1986)

The threshold intensity for excitation of the stimulated Raman backscatter instability has been measured at 9.58 μm in a well-diagnosed plasma free of Brillouin scattering. The initial level of density fluctuations was independently measured by ruby laser scattering. The observed threshold of 1×10^{11} W/cm^2 is somewhat below the calculated "absolute" threshold for underdense plasmas, and the apparent noise level is higher than that measured directly.

I. INTRODUCTION

The harmful effects of stimulated Raman scattering (SRS) in producing energetic electrons in laser fusion work have long been recognized, and indeed this theoretically predicted parametric instability has been indentified in many experiments. Though the SRS thresholds in collisional and collisionless, homogeneous and inhomogeneous plasmas are well known, it has been difficult to verify them experimentally because the local temperature and homogeneity of the plasma, to which the thresholds are sensitive, are usually hard to measure. (The density is also important, but that is easily obtained from the red shift of the reflected light.)

In part II of this paper,[1] we show that a number of previous experiments appear to give thresholds below the theoretical ones, and we reconsider the theory of SRS to see if the predictions can be reconciled with the observations. In this paper (I), we report a measurement made close to but below the so-called "absolute" threshold in a dissipative plasma. This experiment differs from previous ones[2] in combining four important features. First, the competing process of stimulated Brillouin scattering, present in all other experiments, has been eliminated by the use of a plasma with $T_i/T_e > 1$. Second, the density scale length L_n was measured by dual-axis ruby laser interferometry, and the scattering was done at the density minimum, where the threshold is relatively insensitive to L_n. Third, filamentation of the beam was suppressed by using a highly underdense plasma. And fourth, the initial level of fluctuations at the plasma frequency was measured by Thomson scattering.

II. APPARATUS

A schematic of the experimental setup is shown in Fig. 1. The plasma is independently created by a fast θ pinch connected to a 11.1 μF capacitor bank by a parallel-plate transmission line, resulting in a ringing time of 4.3 μsec. Under normal operating conditions the bank is charged to 28.5 kV (4.5 kJ), giving 460 kA maximum current. The single-turn coil, 10 cm i.d. and 22.5 cm long, has a 2.5 cm gap at the midplane for diagnostics. The quartz discharge tube is 7.5 cm i.d. and has three 2 cm i.d. ports at the midplane. No preionization or bias field is used, and the gas is helium. Pinch timing is monitored with a photodiode viewing the visible radiation from the central experimental region. The photodiode signal reaches a peak about 550 nsec after gas breakdown occurs at the wall. At this time the shock front has reached the axis, and the plasma is at its first compression, as confirmed by extensive holography at various times. The scattering is done at this first compression, hereafter defined as $t = 0$. The magnetic field is about 15 kG at this time and does not reach its maximum of 24 kG until later. The $\beta = 1$ plasma, however, screens this field from the plasma on axis, as will be seen from the interferograms. A second maximum in the photodiode signal occurs at $t \simeq 350$ nsec, when the temperature will be higher and the SRS undetectable.

The CO_2 laser system is the same as that used previously for studies of Brillouin scattering[3] except that an SF_6 cell was used in the oscillator to produce radiation of 9.58 μm instead of 10.6 μm. This wavelength was chosen because of the availability of filters that could reject unshifted light and pass Raman-scattered light redder than 10 μm. A grating after the oscillator was used to suppress self-lasing. The incident pulse, $\lesssim 50$ nsec FWHM in duration, is focused axially into the pinch by an $f/7.2$ ZnSe lens and has a peak intensity of 3.4×10^{11} W/cm^2 in a 300 μm diameter spot. Unscattered light is absorbed by a Plexiglas window.

The backscattered light passes through the focusing lens and is partially reflected by a NaCl beam splitter, collimated into a parallel beam smaller than the spectrometer grating, frequency analyzed, and focused onto a Cu:Ge detector at 4.2°K. To decrease the sensitivity of alignment, the grating can be replaced by a mirror and a series of filters. Calibration of the spectrometer was verified by varying the plasma density and hence the SRS red shift. Rejection of unshifted and Brillouin-scattered light was measured to be greater than a factor of 10^8.

III. PLASMA DIAGNOSTICS

A. Plasma density

The density $n_e(\mathbf{r})$ was measured by simultaneous end-on and side-on holographic interferometry using a 25 nsec pulsed ruby laser in the arrangement shown in Fig. 2. The uniformity of the plasma at the first compression is indicated by the end-on views, taken without a hollow wedge, as exemplified by Fig. 3. The absence of fringes in the central region gives an upper limit to the radial density gradient and, hence, to any trapped magnetic field in the experimental region. Since the path length in the axial view is ill defined, the absolute density could not be determined by axial interferometry

[a] Physics Department, 1-130 Knudsen Hall.
[b] Electrical Engineering Department, 7731 Boelter Hall.

 0031-9171/86/113864-09$01.90

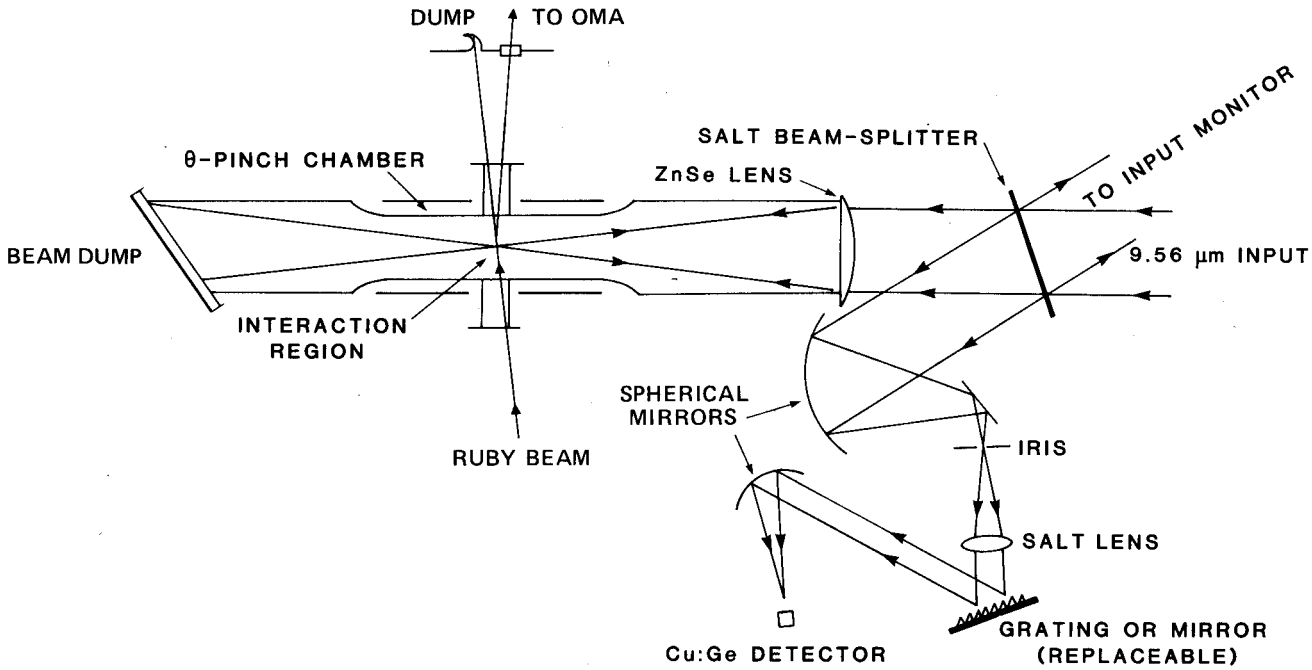

FIG. 1. Diagram of the experiment.

alone. Nonetheless, an estimate of plasma length based on magnetic field shape yielded a value of n_e within 10% of that obtained from side-on interferometry; namely $n_e \simeq 5-6\times10^{16}$ cm^{-3}. Figure 4 shows an example of a side-on view using the standard technique of double exposure with and without plasma, and vacuum fringes produced with a hollow wedge. Abel inversion of these fringe shifts was done with a knowledge of the general shape of density profile measured axially. A check was made by employing the following reverse procedure. First the measured[4] profile $n(r)$ was obtained from the axial interferograms by fitting a seventh-degree polynomial. Using this profile, expected radial fringe patterns were generated by computer and then compared with the measured ones to obtain the absolute density. The axial scale length L_n was obtained by plotting the density across the 2 cm clear aperture of the side port and fitting to a parabola of the form $n_e = n_0(1 + z^2/L_n^2)$. This yielded the scale length L_n of 15 cm used in the analysis of the SRS data.

B. Electron temperature

The value of T_e in the θ pinch varies with charging voltage, pressure, and time. It was measured by the ratio of the He II 4686 Å and He I 5876 Å line intensities, and by the 4686 Å-to-continuum ratio. Both methods yielded a value of 8–12 eV at the time of the first compression. At later times, such at $t = 350$ nsec, when the magnetic field is near its maximum, T_e rises to $\simeq 35$ eV. The time-resolved temperatures during the 50 nsec CO_2 laser pulse, however, could not be obtained; these are calculated in the next section.

C. Ion temperature

The ion temperature was estimated by three methods, all of which were in rough agreement.

(1) The line shape of He II 4686 Å, if due to a simple convolution of Stark and Doppler broadening, yields a value $T_i \simeq 70$–90 eV.

(2) Assuming that plasma and magnetic field pressures are balanced at the time of maximum field ($t = 350$ nsec),

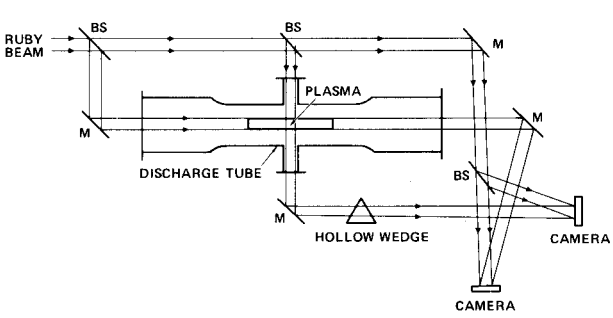

FIG. 2. Setup for dual axis interferometry.

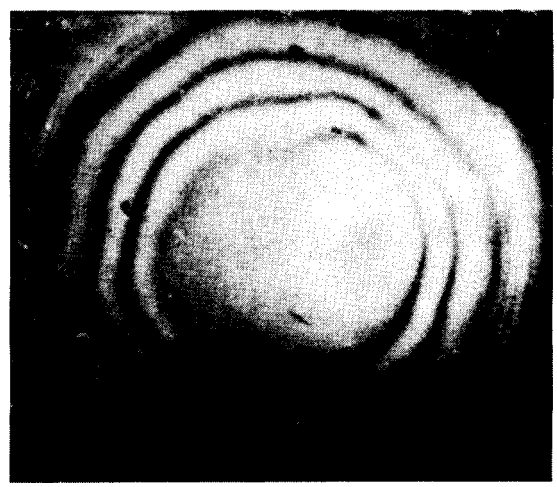

FIG. 3. Axial ruby interferogram of plasma at first compression. Diameter of region within the first fringe is 0.5 cm.

FIG. 4. Radial ruby interferogram from which the density scalelength was measured. The magnetic field is parallel to the fringes.

one can obtain from the measured values of B, n_e, and T_e a value of $T_i \simeq 60$–90 eV.

(3) The directed kinetic energy of the ions acquired during implosion can be calculated from the radius and time of the first compression. Assuming that this energy is thermalized to give the ion temperature, we obtain $T_i \simeq 70$ eV. The exact value of T_i is unimportant; what matters is that all these methods yield $T_i > T_e$. Under this condition, ion waves are heavily Landau damped, and Brillouin scattering should not occur. Indeed, it was not seen.

IV. CALCULATED CONDITIONS

The following plasma conditions could not be measured and had to be calculated.

A. Laser heating

With an initial electron temperature T_0 of $\simeq 10$ eV, the power of the CO_2 beam is sufficient to heat the plasma significantly during the 50 nsec pulse width. To calculate the inverse bremsstrahlung absorption, we first assume that the focal region is so long and thin that the primary heat loss is via radial heat conduction. The electron temperature then follows the heat flow equation

$$\frac{3}{2}nk\frac{\partial T_e}{\partial t} - \frac{1}{r}\frac{\partial}{\partial r}\left(rK_{\|}\frac{\partial T_e}{\partial r}\right) = Q, \tag{1}$$

where the collisional absorption rate in an underdense plasma is[5]

$$Q = 9700(\lambda_\mu/10.6)^2 Z n_{16}^2 I_w \ln\Lambda(\nu) T^{-3/2} \text{ ergs/cm}^3 \text{ sec} \tag{2}$$

and λ_μ is the laser wavelength in μm, Z is the ion charge number, n_{16} is $10^{-16} n_e$, I_w is I_0 in W/cm^2, $\ln\Lambda(\nu)$ is the high-frequency Coulomb logarithm, and T is KT_e in eV. For CO_2 radiation, Λ is approximately $\Lambda \simeq 5T$. Since $\omega_c \ll \nu_{ei}$ is obeyed in the focal region, heat conduction is unimpeded by any magnetic field; and we employ the parallel heat conductivity given by

$$K_{\|} = 0.026 T^{5/2}/Z \ln\Lambda \text{ W/cm-°K}, \tag{3}$$

with $\ln\Lambda$ having its low-frequency value. The last three equations give

$$T^{3/2} n_{16}\frac{\partial T}{\partial t} - \frac{126\,000}{Z\ln\Lambda}\frac{T^{3/2}}{r}\frac{\partial}{\partial r}\left(rT^{5/2}\frac{\partial T}{\partial r}\right) = 0.4Z(\lambda_\mu/10.6)^2 n_{16}^2 I_w \ln\Lambda(\nu). \tag{4}$$

The steady-state solution is given by

$$\frac{1}{r}T^{3/2}\frac{\partial}{\partial r}\left(rT^{5/2}\frac{\partial T}{\partial r}\right) = -3.2\times 10^{-6} Z^2\left(\frac{\lambda_\mu}{10.6}\right)^2 \times n_{16}^2 I_w \ln(\Lambda)\ln\Lambda(\nu). \tag{5}$$

The temperature distribution for $r < a$, where a is the beam radius, is not easily obtained, and in any case $I_w(r)$ is not accurately known. In the exterior region $r > a$, however, the source term on the right-hand side vanishes, and the solution is

$$T^{7/2}(r) - T_0^{7/2} = C\ln(R/r), \tag{6}$$

where T_0 is the temperature at some large radius R. The constant C can be found by matching heat fluxes at the boundary $r = a$. The central temperature $T(0)$ will be only slightly higher than $T(a)$. The heat flux across the surface $r = a$ is given by

$$\pi a^2 \overline{Q} = -2\pi a K_{\|} T'_a, \tag{7}$$

where $\overline{Q}$ is the average heat absorption in the focus. The value of $T'(a)$ found from Eq. (6) is

$$T'(a) \equiv T'_a = -\tfrac{2}{7}(C/a)T_a^{-5/2}. \tag{8}$$

Equations (2), (3), (5), (7), and (8) then determine C in terms of the plasma parameters. Writing P_{MW} for $10^{-6}\pi a^2 I_w$, we obtain the solution

$$T_a^{3/2}(T_a^{7/2} - T_0^{7/2}) = 1.79(\lambda_\mu/10.6)^2 Z^2 n_{16}^2 P_{MW} \ln\Lambda \times \ln\Lambda(\nu)\ln(R/a). \tag{9}$$

The radius R at which T falls to nearly the initial value T_0 is not known, but Eq. (9) is very insensitive to it. If we take $R/r \simeq 10$, $\lambda_\mu \simeq 10.6$, and neglect $T_0^{7/2}$, which usually gives only a small correction, we obtain the useful formula

$$T^5 \simeq 4Z^2 n_{16}^2 P_{MW} \ln\Lambda \ln\Lambda(\nu). \tag{10}$$

For our experimental parameters of $n_e = 8\times 10^{16}$ cm^{-3}, $T_0 = 10$ eV, $P_{MW} \simeq 200$, $\ln\Lambda \simeq 7$, $\ln\Lambda(\nu) \simeq 4$, and $Z \simeq 2$, Eq. (9) gives $T(a) \simeq 20$ eV. Since P_{MW} varies by a factor of 3 and $T(0)$ is somewhat larger than $T(a)$, the laser-heated electron temperature in the experiment should be around 17–21 eV.

The heating rate can be obtained from Eqs. (1) and (2) by neglecting the conduction term. We then obtain

$$\frac{2}{5}\frac{\partial T^{5/2}}{\partial t} = 0.4Z\left(\frac{\lambda_\mu}{10.6}\right)^2 n_{16} I_w \ln\Lambda(\nu), \tag{11}$$

whose solution is

$$T_a(t) = [T_0^{5/2} + 1.0Z(\lambda_\mu/10.6)^2 n_{16} I_{MW} \ln\Lambda(\nu) t_{\mu\text{sec}}]^{2/5} \text{ eV}. \tag{12}$$

For a pulse width $t = 0.05$ μsec and an average intensity $I_0 = 1.5\times 10^5$ MW/cm^2, Eq. (12) gives $T(a) = 130$ eV. There is therefore ample time to reach the conduction-limited temperature of $T_e \simeq 20$ eV during the laser pulse.

Laser heating also affects the rate of heat transfer from the ions. In the θ-pinch equilibrium, electron–ion collisions result in temperatures of $T_i \simeq 80$ eV, $T_e \simeq 10$ eV. When T_e is raised to, say, 20 eV by laser heating, the electron–ion equilibration time τ_{eq} is increased and $T_i - T_e$ is decreased, so that the heat flow from the ions is reduced. The heat flow is given by $Q_{ie} = 1.5 n_e (KT_i - KT_e)/\tau_{eq}$, which maximizes at 3.5×10^7 W/cm^2 at $T_e = 10$ eV for $Z = 2$, $n_e = 8\times10^{16}$ cm^{-3}. The heat input from inverse bremsstrahlung, given by Eq. (2), is at least 1.25×10^9 W/cm^3 (at $I_0 = 10^{11}$ W/cm^2, $T_e = 10$ eV). The change in ion heating, therefore, is negligible.

B. Degree of ionization

Since helium was used, there is some uncertainty as to the value of $\bar{Z}$. If coronal equilibrium obtains, the value of T_e for $\bar{Z} = 1.5$ is[6] $\simeq 7$ eV. Hence, at the initial temperature of $\simeq 10$ eV, and certainly at the laser-heated temperature of $\simeq 20$ eV, the helium should be completely stripped. This is consistent with the filling pressure of 85 mT, which gives an initial neutral density of 2.8×10^{15} cm^{-3}. Assuming that this gas is all ionized and compressed by the measured volume compression ratio of 9, we obtain an electron density $\bar{n}_e$ of 5×10^{16} cm^{-3} for $Z = 2$. This agrees with the value 6×10^{16} cm^{-3} measured interferometrically and also with the more exact value of 8×10^{16} cm^{-3}, deduced from the SRS red shift, for the peak density on axis.

C. Filamentation and self-focusing

The conditions for filamentation have been given by Kaw *et al.*[7] for the case of steady-state balance between the plasma pressure and the ponderomotive force of a striated laser beam. Let the plasma have plane ripples of wavelength λ_f and wavenumber k_f in the direction perpendicular to $\mathbf{E}_0$ (the worst case). The growth length of the one-dimensional "filaments" is then given by L_f, where

$$\frac{1}{L_f^2} = k_f^2\left(\tfrac{1}{2}\frac{n_0}{n_c}\beta E_0^2 \exp(-\beta E_0^2) - \frac{k_f^2}{4k_0^2}\right), \tag{13}$$

$$\beta \equiv Ze^2/4m\omega_0^2[ZKT_e + KT_i]. \tag{14}$$

Figure 5 shows L_f as a function of λ_f, as computed from Eq. (13) with $\lambda_0 = 9.58$ μm, $T_e = 19$ eV, $T_i = 80$ eV, $n_0 = 8\times10^{16}$ cm^{-3}, and $I_0 = 1$ and 3×10^{11} W/cm^2. It is clear that even the highest available intensity ($\beta E_0^2 = 2.6\%$) is not sufficient to excite filaments of wavelength shorter than the focal diameter of 300 μm.

Whole beam self-focusing is not well represented by Eq. (13) but has been studied for cylindrical beams of Gaussian profile by Max.[8] If a beam is injected at the right angle into a preformed density channel, the beam radius can be maintained at an equilibrium value a_e at which diffraction just balances self-focusing. The radius a_e is given by[8]

$$a_e^2 = 2(c/\omega_p)^2/\beta E_0^2 \exp(-\beta E_0^2). \tag{15}$$

For $\beta E_0^2 = 0.026$, this yields $a_e = 167$ μm, approximately the same as the initial radius. On the other hand, if the beam has arbitrary radius a_0 and spherical wave fronts of radius R_0 as it enters the plasma, it either focuses to a minimum radius

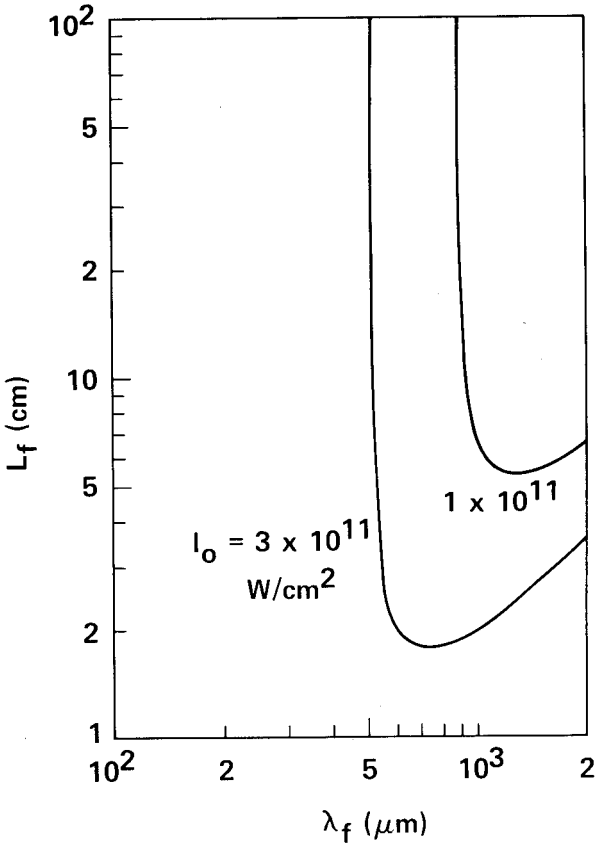

FIG. 5. Filamentation growth length L_f versus ripple wavelength λ_f for conditions of the present experiment.

a_m and then diverges, or it oscillates between a_m and a maximum radius a_m'. The radii are given by the equation[8]

$$y^2 + \frac{a_0^2\omega_p^2}{2c^2}\left(e^{-\beta E_0^2 y^2} - e^{-\beta E_0^2}\right) = 1 + \frac{k_0^2 a_0^4}{4R_0^2} \equiv y_{vac}^2, \tag{16}$$

where $y \equiv a_0/a_m$ and ω_p is the undisturbed plasma frequency. The oscillating and one-bounce solution occur when y_{vac}^2 is greater than or less than the left-hand side when $y = 0$. For this experiment the former condition obtains, and the minimum radius is found by solving Eq. (16) for the larger value of y. To evaluate y_{vac}, we note that the focusing lens has f number $R_0/2a_0 = 7.2$, so that $a_0 = R_0/14.4$. Assuming that the dense plasma extends 10 cm from the midplane, we take $R_0 = 10$ cm and $a_0 = 0.7$ cm. Then $y_{vac} = 158$ and $a_{vac} = a_0/y_{vac} = 44$ μm. Thus, the measured radius of $\simeq 150$ μm is about three times the diffraction limit. For $\beta E_0^2 = 0.026$ and $y > y_{vac}$, the term $\exp(-\beta E_0^2 y^2)$ is negligible, and Eq. (16) becomes

$$\frac{y^2}{y_{vac}^2} = 1 + \frac{a_0^2\omega_p^2}{2c^2 y_{vac}^2} e^{-\beta E_0^2} \simeq 1 + \frac{2}{k_0^2 a_0^2}\frac{R_0^2\omega_p^2}{c^2} e^{-\beta E_0^2}. \tag{17}$$

For our parameters, $y^2/y_{vac}^2 = 3.7$, so that I_0 can be increased at least a factor 3.7 over its vacuum value by self-focusing. The self-focusing distance is given by[8]

$$L_{sf} = \pi k_0 (c/\omega_p)^2 e^{\beta E_0^2}/\sqrt{2}(\beta E_0^2)^{3/2}. \tag{18}$$

As I_0 varies from 1 to 3×10^{11} W/cm^2, L_{sf} decreases from 64 to 13 cm, comparable to R_0. Thus, there is a possibility that, at the highest intensities, I_0 is $\simeq 4$ times larger than assumed, making the saturation of the growth curve more severe than is shown later in Fig. 10. Note that Eq. (17) predicts a decrease of self-focusing as I_0 increases. This is due to the emptying of the density channel to such an extent that the light is no longer refracted. That this does not happen here [because $1-\exp(-\beta E_0^2)$ is only 2.6% at the highest I_0] is corroborated by the fact that the SRS red shift gives a value of n_0 close to that measured by interferometry.

In addition to ponderomotive self-focusing, there is also thermal self-focusing, which depends on the temperature gradient inside the beam. We have solved for this from Eq. (5) assuming a Gaussian profile and have found that ponderomotive self-focusing dominates; the details are omitted.

V. MEASUREMENT OF NOISE LEVEL

In comparing theory with experiment on convective instabilities, the initial level of fluctuations is needed and is usually unknown. In this experiment, we have measured it by ruby laser Thomson scattering, passing the 6943 Å probe beam via a midplane port through the experimental region at the CO_2 laser focus. Since the $\mathbf{k}$ of the plasma waves in question is known to be $\mathbf{k}\simeq 2\mathbf{k}_0$, one can calculate the scattering angle to be $\theta\simeq\sin^{-1}(0.69/4.79)=8.3°$. The scattering parameter in this case is $\alpha\equiv 1/k\lambda_D = 9.2$ at $n=8\times10^{16}$ cm^{-3} and $T_e = 10$ eV, well into the collective regime. The transmitted beam is dumped, the scattered light collected by a window and lens and then focused onto the slit of a spectrograph, and the one-discharge scattered spectrum is recorded by an optical multichannel analyzer (OMA). By introducing an attenuating filter in front of the OMA channels covering the unshifted frequency, it was possible to record both the scattered light and the stray light on the same discharge. Both blue-shifted and red-shifted plasma satellites should be seen on either side of the stray light peak. However, because of the interference of an ionized He line with the blue peak, only the red satellite was measured. An example of such a spectrum, taken under standard conditions at the first compression of the θ pinch and with no incident CO_2 beam, is shown in Fig. 6(a). The width of the plasma satellite is mostly instrumental, the plasma being uniform in density over most of the scattering length. The position of this peak gives the Bohm–Gross frequency on axis to within 2%. The effects of plasma heating on the plasma satellite is shown in Figs. 6(b) and 6(c). In Fig. 6(b), the ruby pulse is delayed until the magnetic field is at maximum, when T_e has risen to $\simeq 35$ eV. In Fig. 6(c), the CO_2 laser is fired, heating the plasma to the calculated temperature of $\simeq 19$ eV and also exciting SRS during part of the pulse. The position of the peak shifts with the density when the filling pressure is varied.

Using calibrated filters, the power scattered into the collecting optics, integrated in frequency over the electron feature, was measured relative to the incident ruby power. Under standard conditions, the result is

$$(P_s/P_0)\quad(\text{ruby}) = 2.3\times10^{-13}\quad(\text{measured}). \tag{19}$$

The number increased in rough proportionality to T_e when measured at later times in the θ pinch pulse. How this number is related to the initial density fluctuation is not straightforward and requires discussion.

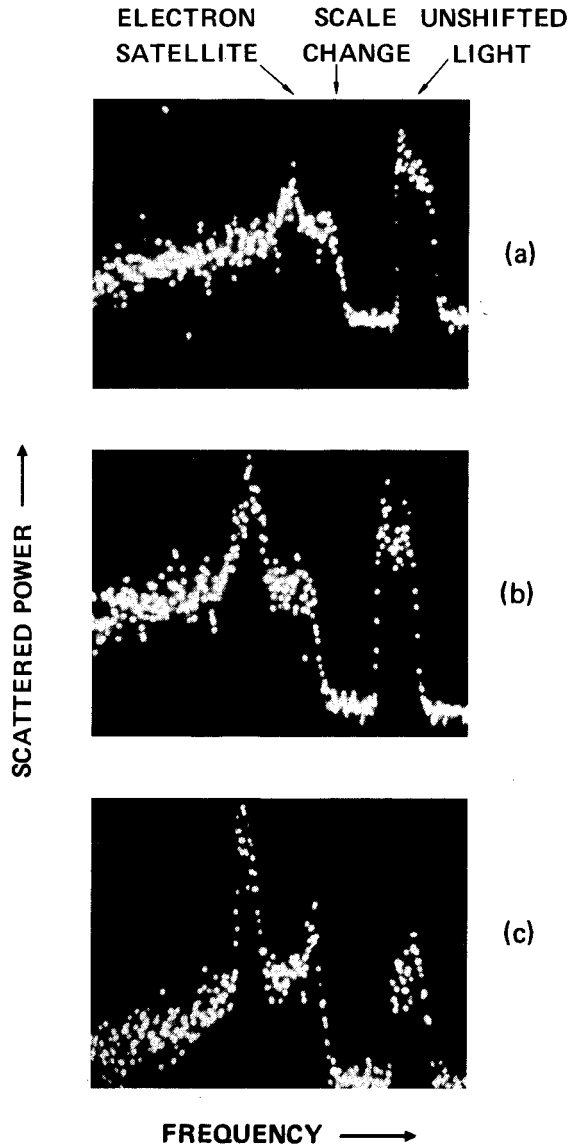

FIG. 6. Spectra of Thomson scattered light. (a) Spectrum of ruby light scattered by the theta pinch plasma (with no CO_2 beam), showing the electron feature redshifted by $\simeq\omega_p$. The sharp drop in background radiation at the right is caused by a filter used to suppress the stray light peak. (b) The same at a later time, when T_e is higher. (c) The same with the CO_2 laser on.

We first calculate the expected scattering from a thermal plasma with $n_e = 8\times10^{16}$ cm^{-3}, $T_e\simeq 10$ eV, and diameter $\simeq 0.5$ cm, as measured by axial interferometry. The scattering geometry for both the ruby and CO_2 beams is shown in Fig. 7. The collecting window for Thomson scattering subtends a solid angle $\Delta\Omega = 8.3\times10^{-3}$ sr centered at $\theta = 8.3°$; this is the only limiting element in the optical system. The theoretical Thomson-scattered power is given by[9]

$$P_s/P_0 = n_e r_0^2 L\,\Delta\Omega\,S(\mathbf{k})/2\pi, \tag{20}$$

where $r_0 = e^2/mc^2 = 2.82\times10^{-13}$ and $S(\mathbf{k})$ is the frequency-integrated scattering function for the electron feature,

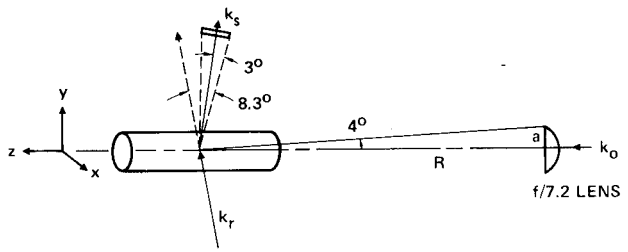

FIG. 7. Scattering geometry for ruby Thomson and CO_2 Raman scattering from plasma waves. The angles are exaggerated.

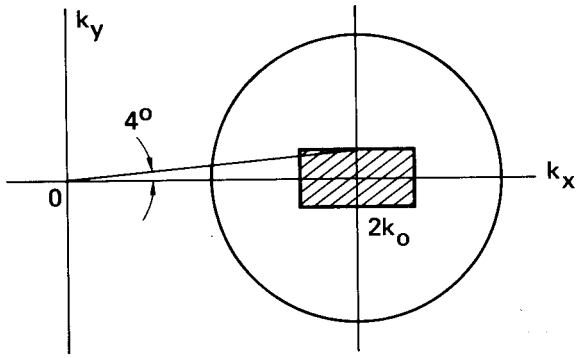

FIG. 8. The range of **k** measured by ruby Thomson scattering and the part (shaded area) of this which contributes to SRS.

given by

$$S(\mathbf{k}) = \tfrac{1}{2}\times 2\pi/(1+\alpha^2). \tag{21}$$

We have included a factor $\frac{1}{2}$ to account for the loss of the blue satellite. Taking $L = 0.5$ cm and $\alpha = 9.175$, we find $S(\mathbf{k}) = 3.69\times 10^{-2}$ and

$$P_s/P_0 = 1.5\times 10^{-13} \quad \text{(thermal)}. \tag{22}$$

Thus, the measured level is 1.5 times thermal, or essentially thermal within the experimental error. This is the level appropriate to the measured SRS threshold, which occurs at intensities too low for laser heating to be significant.

For future reference we also calculate the thermal Thomson scattering of the CO_2 beam. The focusing lens (Fig. 7) subtends a solid angle $\Delta\Omega = 1.5\times 10^{-2}$ sr, and $S(\mathbf{k})$ remains the same if we consider **k**'s near $2\mathbf{k}_0$. The scattering length L is now determined by the distance from the midplane where the incident beam diameter becomes larger than the 0.5 cm diameter of uniform, high-density plasma. This occurs at $z = 3.6$ cm. Adding a small amount for scattering from the low-intensity region beyond this, we take $L \simeq 10$ cm. Equation (20) then gives

$$P_s/P_0 \quad (CO_2) = 5.6\times 10^{-12} \quad \text{(thermal)}. \tag{23}$$

If the fluctuation level is 1.5 times thermal, Raman scattering would start from the reflectivity

$$R = P_s/P_0 \quad (CO_2) = 8.4\times 10^{-12} \quad \text{(expected)}. \tag{24}$$

To calculate the corresponding density fluctuation we use the theory of Bragg scattering, which gives, for the intensity integrated over a diffraction peak[10]

$$P_s/P_0 = (\tfrac{1}{2}r_0\lambda_r n_1 L)^2. \tag{25}$$

λ_r being the ruby wavelength and n_1 the peak amplitude of a density fluctuation of given **k** and ω satisfying the matching conditions. The number of wavelengths of $n_1(\mathbf{k},\omega)$ measured depends on the ruby spot size ($\simeq 200\,\mu$m); this gives rise to a finite spread of the scattered beam which is well covered by the collection optics. However, the defining aperture also accepts light scattered from fluctuations of other **k**'s, some of which are not relevant to the SRS noise source. We assume that ω matching is exact; in any case, we integrate over the ω spectrum of the plasma satellite. By using the well-known relation

$$2\sin(\theta/2) = k/k_r, \tag{26}$$

we can map the range of θ covered by the collection window (Fig. 7) into a circle in k_x-k_y space, as shown in Fig. 8. The circle is centered at $(2k_0, 0)$ and has radius 4.6×10^3 cm^{-1}.

The range of k_y contributing to observed SRS is determined by the 4° half-angle of the focusing lens (Fig. 7); this gives a range $\Delta k_y \simeq 0.87\times 10^3$ cm^{-1}. There is also a range Δk_x for SRS; we shall find in the Appendix that $\Delta k_x \simeq 1.7\times 10^3$ cm^{-1}. The shaded area in Fig. 8 has $k_y = \pm\Delta k_y$, $k_x = 2k_0 \pm \Delta k_x$ and represents the range of k's contributing to SRS. We assume that the plasma is completely turbulent, so that the scattered intensity at neighboring k's is uncorrelated. In a thermal plasma, $S(\mathbf{k})$ is proportional to $\simeq 1/\alpha^2 \propto k^2 KT_e$ and independent of direction. In the θ-pinch plasma, $S(\mathbf{k})$ is nearly thermal and has been found to have approximately the same T_e dependence. It is reasonable to assume $S(\mathbf{k}) \propto k^2$ here, but in any case we can obtain the right order of magnitude even if the k dependence is neglected. Then the fraction of P_s/P_0 that contributes the SRS noise source is ratio of the areas of the rectangle and the circle in Fig. 8. This ratio is 0.09. Multiplying Eq. (19) by 0.09 and using this in Eq. (25), we obtain

$$n_1/n_0 = 3.6\times 10^{-7}. \tag{27}$$

VI. RESULTS AND DISCUSSION

The Raman backscatter radiation collected as shown in Fig. 1 appears in short spikes of $\simeq 2$ nsec width, usually one per pulse, but sometimes 3 or 4. Figure 9(a) shows an example of a single spike superimposed on the photodiode plasma light signal and the CO_2 pulse monitor (delayed by 150 nsec), showing the relative timing. Figure 9(b) shows a discharge with three SRS spikes. These signals appear only in a window of time 80 nsec wide during the first compression of the θ pinch, and only at the peak of the CO_2 pulse. These observations are consistent with the picture given below that laser heating is required to bring the SRS threshold below the available intensity, and that at subsequent compressions of the θ pinch the electron temperature is too high and the plasma waves are Landau damped. The spectrum of the scattered light is peaked at $\lambda = 10.46 \pm 0.06\,\mu$m, corresponding to $n_e = 8\times 10^{16}$ cm^{-3}.

That stimulated Brillouin scattering (SBS) has been eliminated by ion Landau damping ($T_i/T_e \simeq 4$) was verified by tuning the backscatter spectrograph grating to accept unshifted light near 9.58 μm. The expected acoustic shift of 100 GHz falls well within the range covered by the detector. No

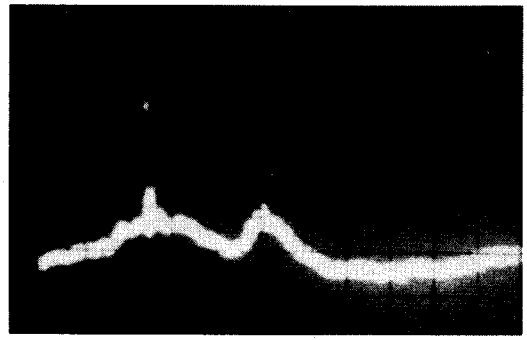

(a)

(b)

FIG. 9. Examples of SRS spikes seen on the backscatter detector. In (a) the plasma light monitor and the CO_2 input pulse are superimposed, with the latter intentionally delayed by 150 nsec. Sweep speed: 100 nsec/div. In (b) three spikes appear on the same discharge; 5 nsec/div.

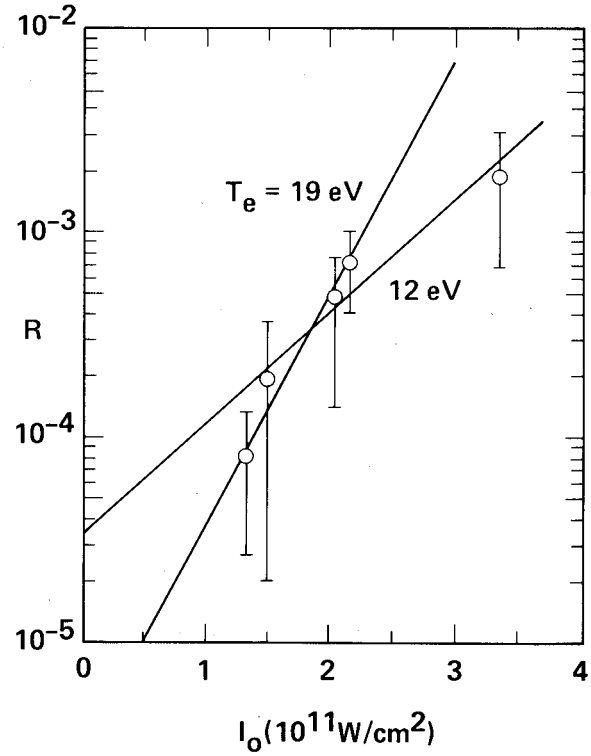

FIG. 10. SRS power reflectivity versus I_0. The error bars show the standard deviation in averaging over discharges. The lines indicate the expected slopes at various T_e provided that the instability is in the collisional, convective regime.

SBS was detected at levels down to 10^{-3} of the SRS signal at any time during the laser pulse.

The SRS power reflectivity $R = P_s/P_0$ (CO_2) was measured by taking the peak height of each spike and averaging over many pulses. The absolute value was obtained by using calibrated beam splitters and attenuators. Fig. 10 shows the growth curve R vs I_0. The lowest intensity at which SRS signals were seen was $I_0 = 1.3\times10^{11}$ W/cm^2. We next discuss how this compares with the expected threshold.

Conventional theories of SRS[11,12] predict that (1) absolute instability in an infinite, homogeneous, underdense plasma and (2) convective instability in a homogeneous plasma of finite length L both require

$$\gamma_0^2 > \frac{V_1 V_2}{4}\left(\frac{\gamma_1}{V_1}+\frac{\gamma_2}{V_2}\right)^2 \equiv \gamma_a^2, \tag{28}$$

where, from Eqs. (A5) and (A6),

$$\gamma_0^2 = a_1 a_2 \simeq 3.44 I_0 \lambda_0 \omega_p, \tag{29}$$

for $\omega_p^2 \ll \omega_0^2$ and I_0 in W/cm^2. In Eq. (28), the group velocity V_1 is given by Eq. (A7), and V_2 is essentially c. Figure 11 shows the "absolute" threshold γ_a, expressed in terms of I_0, plotted against T_e for the well-determined density of 8×10^{16} cm^{-3}, and $Z = 1$ and 2. In evaluating Eq. (28), γ_2/V_2 was always negligible, and γ_1 was taken to be the sum of Landau and electron-ion collisional damping. The exact expressions used are given in Ref. 1. The minima in Fig. 11 occur where

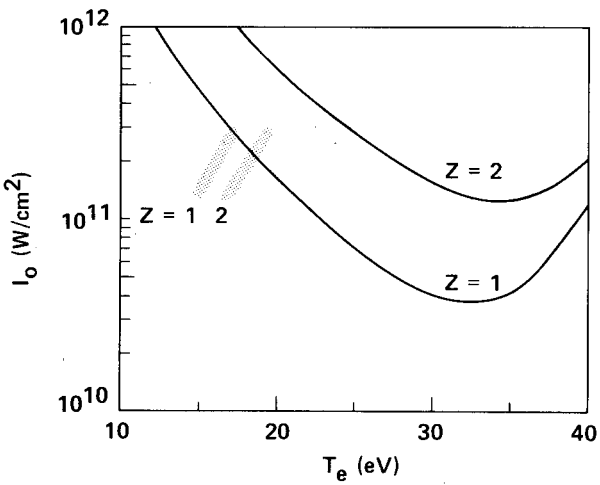

FIG. 11. The "absolute" threshold intensity versus T_e for $n_e = 8\times10^{16}$ cm^{-3} and $\lambda_0 = 9.58\,\mu$m. The shaded bars indicate the ranges where SRS was observed if $Z = 1$ or 2, where Z is the ionization state of the He gas.

collisional and Landau damping are equal; collisions dominate at lower T_e, and Landau damping at higher T_e. Also shown in Fig. 11 is the range of I_0 in which SRS was detected (Fig. 10), plotted against the value of T_e calculated from Eq. (9) assuming either $Z=1$ or 2. If ionization equilibrium is reached, the experimental conditions should be close to $Z=2$. It is seen that the observed threshold of $I_0 = 1.3\times10^{11}$ W/cm^3 lies below the theoretical curve, and there is agreement only at the highest available intensity (3×10^{11} W/cm^3) and only if one assumes $Z=1$. If I_0 is increased a factor of 4 by self-focusing, T_e is unchanged because it depends on P_0, not I_0; and the experimental range should be moved upwards. Agreement between theory and experiment is then quite close if $Z=1$ and is reached for $Z=2$ for $I_0 > 2\times10^{11}$ W/cm^2. However, at $I_0 = 1$–2×10^{11} W/cm^2, Eqs. (17) and (18) show that self-focusing cannot increase I_0 as much as a factor of 4, this factor being possible only for $I_0 = 3\times10^{11}$ W/cm^2. From these considerations we conclude that SRS was observed at intensities somewhat below the absolute threshold, but within a factor 2–10 of it.

When $\gamma_0 < \gamma_a$, convective SRS is still possible when the plasma wave damping γ_1 is not small. To calculate the amplification factor, we make the simplification that the inhomogeneous plasma can be approximated by a homogeneous plasma of finite length L, that length being the distance between turning points in the inhomogeneous plasma problem.[13] Since our experiment is performed at a density minimum, we have calculated L for a parabolic profile of the form $n_e = n_{e0}(1 + z^2/L_n^2)$, with the result[14]

$$L = (18 k_0 L_n^2 \lambda_D^2)^{1/3}. \tag{30}$$

The reflected power P_s is then given in terms of the noise power P_n by[12,13,15]

$$P_s = P_n e^{2N}, \tag{31}$$

where

$$N = \gamma_0^2 L / c\gamma_1. \tag{32}$$

Equations (29), (31), and (32) then give the reflectivity

$$R = P_s/P_0 = (P_n/P_0)\exp(6.88 I_0 \lambda_0 \omega_p L / c\gamma_1), \tag{33}$$

with L to be calculated from Eq. (30).

The slope of the growth curve, ln R vs I_0, was computed from Eq. (33) for $n = 8\times10^{16}$ cm^{-3}, $Z=2$, $T_e = 19$ and 12 eV, and $L = 1.5$ mm, which follows from Eq. (30) for $L_n = 15$ cm, as measured in Sec. III. It is seen that, except for the highest intensity point, which could be saturated, the slope is in remarkable agreement with that calculated for the expected temperature of $\simeq 20$ eV. However, this agreement is probably accidental, for two reasons. First, in view of the uncertainty in I_0 due to self-focusing, such close agreement cannot be expected. Second, extrapolation of the 19 eV line to $I_0 = 0$ shows that $P_n/P_0 = 3\times10^{-6}$. This is almost six orders of magnitude larger than the noise level calculated in Eq. (24) from the measured initial density fluctuation. In other words, if $P_n/P_0 = 8.4\times10^{-12}$, Eq. (33) would predict $R = 1.5\times10^{-9}$ at $I_0 = 2\times10^{11}$ W/cm^2, compared with the observed value $I_0 = 5\times10^{-4}$. Thus, the disagreement with theory is not apparent until the initial noise level is independently measured.

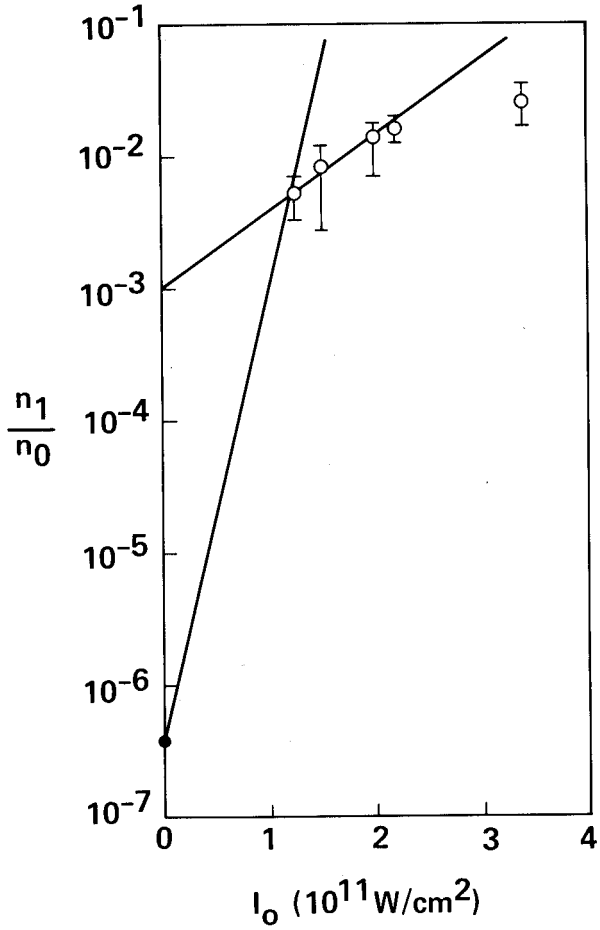

FIG. 12. Plasma wave amplitude n_1/n_0 vs I_0, inferred from the SRS data, and the noise level calculated from the ruby Thomson scattering data. This plot is extremely model-dependent and should be used cautiously.

We may also express the discrepancy in terms of the density fluctuation n_1/n_0. A lower limit to the amplitude of the plasma wave giving rise to the observed R can be estimated by neglecting the spatial variation of n_1 and using the Bragg scattering formula, Eq. (25), which can be rewritten as

$$R = \left(\frac{\pi}{2}\frac{L}{\lambda_0}\frac{n_0}{n_c}\frac{n_1}{n_0}\right)^2. \tag{34}$$

For $R = 5\times10^{-4}$ at $I_0 = 2\times10^{11}$ W/cm^2, we then find $n_1/n_0 = 0.014$, about e^{10} times the noise level estimated in Eq. (27). This is to be compared with the number of e-foldings given by Eq. (32); namely, $N = 2.6$.

The use of Eq. (34) for a wave that should grow exponentially in space may seem inappropriate, but it is not unreasonable for n_1/n_0 to saturate at a few percent as a result of nonlinear frequency shifts, as has been found in experiments on stimulated *Brillouin* scattering.[16] If we use Eq. (34), we can plot the data of Fig. 10 in terms of n_1/n_0, assuming that $L = 0.15$ cm, and compare them with the inferred noise level of Eq. (26). This is shown in Fig. 12. We see that the growth from the noise level increases more rapidly with I_0 than expected, and that the slope beyond threshold, though it agrees with Eq. (33), is probably affected by saturation.

A final possibility is that the experimental conditions

are at the extremes of our estimates of self-focusing and laser heating, or that the collision frequency is anomalously low, in which case all of our points can be above the absolute threshold. The wave packets will then grow in amplitude and length, both of which affect the scattered power. The R vs I_0 curve must then be computed numerically[17] for each case with a knowledge of the initial conditions.

As a result of the knowledge of the initial noise level, which is measured here for the first time, we conclude that SRS has a lower threshold or shorter growth length than conventional theory predicts.

ACKNOWLEDGMENTS

This work was supported by the National Science Foundation, Grant No. ECS 83-10972 and by the Lawrence Livermore National Laboratory, Work Order No. 3446905.

APPENDIX: FORMULATION

We now show that the range of k_x contributing to SRS is $\Delta k_x \simeq 0.13k$. Even if ω matching is exact, a wave packet of finite length can grow out of the noise. Such a wave train contains a range of k values around $2k_0$. This range cannot be too large (the wave train cannot be too short), because off-resonant k's have low growth rate. Hence we must calculate the width of the gain curve $\gamma(k)$. If subscripts 0, 1, and 2 stand for the pump wave, the plasma wave, and the backscattered wave, respectively, the coupled fluid equations for the slowly varying amplitudes E_2 and n_1 are[14]

$$(\omega_2^2 - \omega_p^2 - c^2k_2^2)E_2\cos\Phi_2 - 2(\omega_2\dot{E}_2 + c^2k_2E_2' + \gamma_2\omega_2E_2)\sin\Phi_2 = -\frac{\omega_p^2}{2}\frac{\omega_2}{\omega_0}\frac{n_1}{n_0}E_0\sin(\Phi_2-\delta), \tag{A1}$$

$$(\omega_1^2 - \omega_p^2 - v_e^2k_1^2)n_1\cos\Phi_1 - 2(\omega_1\dot{n}_1 + v_e^2k_1n_1' + \gamma_1\omega_1n_1)\sin\Phi_1 = -\frac{\omega_p^2}{\omega_0\omega_2}\frac{k_1^2}{m}\frac{E_2E_0}{8\pi}\sin(\Phi_1-\delta), \tag{A2}$$

where $\Phi_j = k_jx - \omega_jt$, $v_e^2 = 3KT_e/m$, γ_j are the wave damping rates, and δ is a small angle. To solve for the homogeneous growth rate γ, we set the spatial derivatives E_2', n_1' to zero, replace $\dot{E}_2$ and $\dot{n}_1$ by γE_2 and γn_1, and neglect γ_1, γ_2 relative to γ. We further replace k_j by $k_{j0} + \Delta k_j$, where k_{j0} satisfies the linear dispersion relation. The initial parentheses in Eq. (A1) and (A2) become $-2k_{20}c^2\Delta k_2$ and $-2k_{10}v_e^2\Delta k_1$, respectively. Defining the group velocities $V_2 = c^2k_{20}/\omega_2 \simeq c$ and $V_1 = -v_e^2k_{10}/\omega_1$ (since $k_1 < 0$), and equating the terms with the same time behavior, we obtain the four equations

$$\Delta k_2 = -(a_2n_1/cE_2)\sin\delta, \quad \gamma E_2 = a_2n_1\cos\delta, \tag{A3}$$

$$\Delta k_1 = (a_1E_2/V_1n_1)\sin\delta, \quad \gamma n_1 = a_1E_2\cos\delta, \tag{A4}$$

where

$$a_2 \equiv \omega_p^2E_0/4\omega_0n_0, \tag{A5}$$

$$a_1 \equiv (\omega_p^2k_1^2/2m\omega_0\omega_1\omega_2)(E_0/8\pi). \tag{A6}$$

Multiplying, we obtain

$$\Delta k_1\Delta k_2 = -(\gamma_0^2/cV_1)\sin^2\delta, \quad \gamma^2 = \gamma_0^2\cos^2\delta, \tag{A7}$$

where $\gamma_0^2 \equiv a_1a_2$ is the homogeneous growth rate at exact resonance. Eliminating Δk_2 and δ using Eq. (A3), we obtain

$$\gamma^2 = \gamma_0^2 - V_1^2(\Delta k_1)^2. \tag{A8}$$

The half-width at half maximum of the gain profile $\gamma(k)$ is, therefore,

$$\Delta k = (3/4)^{1/2}(\gamma_0/V_1) \simeq \gamma_0/V_1. \tag{A9}$$

This width varies with pump intensity $I_0 \propto \gamma_0^2$ because it is the nonlinear frequency shift due to the pump which makes excitation possible when the Bohm–Gross relation is not exactly satisfied. Equation (A9) evaluates to $\Delta k/k = 0.13$ for $I_0 = 10^{11}$ W/cm^2, the observed threshold intensity. Thus, $\Delta k/k = 0.13I_{11}^{1/2}$, where $I_{11} = I_0/10^{11}$, and the effective noise level corresponding to $P_s/P_0 = 2.3\times10^{-13}$ (ruby) is

$$n_1/n_0 = 3.6\times10^{-7}I_{11}^{1/2}. \tag{A10}$$

Equation (27) is this formula evaluated at the observed threshold of $I_{11} \simeq 1$.

[1] F. F. Chen, submitted to Phys. Fluids.
[2] R. G. Watt, R. D. Brooks, and Z. A. Pietrzyk, Phys. Rev. Lett. **41**, 170 (1978); A. A. Offenberger, R. Fedosejevs, W. Tighe, and W. Rozmus, *ibid.* **49**, 371 (1982); C. J. Walsh, D. M. Villeneuve, and H. A. Baldis, *ibid.* **53**, 1445 (1984); and others.
[3] M. J. Herbst, C. E. Clayton, and F. F. Chen, Phys. Rev. Lett. **43**, 1591 (1979).
[4] B. Amini, Phys. Fluids **28**, 378 (1985).
[5] T. W. Johnston and J. M. Dawson, Phys. Fluids **16**, 722 (1973).
[6] R. W. P. McWhirter, in *Plasma Diagnostic Techniques*, edited by R. H. Huddlestone and S. L. Leonard (Academic, New York, 1965), p. 207.
[7] P. Kaw, G. Schmidt, and T. Wilcox, Phys. Fluids **16**, 1522 (1973).
[8] C. E. Max, Phys. Fluids **19**, 74 (1976).
[9] J. Sheffield, *Plasma Scattering of Electromagnetic Radiation* (Academic, New York, 1975), p. 157.
[10] L. D. Landau and E. M. Lifshitz, *Electrodynamics of Continuous Media*, (Pergamon, Oxford, 1960), Chap. XV. A factor $\frac{1}{4}$ has been added to the x-ray diffraction result to account for our omission of the blue satellite.
[11] C. S. Liu, M. N. Rosenbluth, and R. B. White, Phys. Fluids **17**, 1211 (1974).
[12] D. W. Forslund, J. M. Kindel, and E. L. Lindman, Phys. Fluids **18**, 1002 (1975).
[13] F. F. Chen, in *Laser Interaction and Related Plasma Phenomena*, edited by H. J. Schwartz and H. Hora (Plenum, New York, 1974), Vol. 3A, p. 291.
[14] See AIP document No. PAPS PFLDA-29-3864-29 for 29 pages of UCLA Report No. PPG-746 by B. Amini and F. F. Chen (1976). Order by PAPS number and journal reference from American Institute of Physics, Physics Auxiliary Publication Service, 335 East 45th Street, New York, NY 10017. The price is $1.50 for each microfiche (98 pages) or $5 for photocopies of up to 30 pages, and $.15 for each additional page over 30 pages. Airmail additional.
[15] D. Pesme, G. Laval, and R. Pellat, Phys. Rev. Lett. **31**, 203 (1973).
[16] C. E. Clayton, Ph. D. thesis, University of California, Los Angeles, 1984.
[17] M. N. Rosenbluth, R. B. White, and C. S. Liu, Phys. Rev. Lett. **31**, 1190 (1973).